Article

Cite This: *Biomacromolecules* XXXX, XXX, XXX−XXX

pubs.acs.org/Biomac

Enhanced Arylamine *N*-Oxygenase Activity of Polymer−Enzyme Assemblies by Facilitating Electron-Transferring Efficiency

Libo Zhang, Yanmei Xu, Thomas M. Makris,* and Qian Wang*

Department of Chemistry and Biochemistry, University of South Carolina, 631 Sumter Street, Columbia, South Carolina 29208, United States

Supporting Information

ABSTRACT: A novel *N*-oxygenase-coated core−shell nanoparticle was generated through the coassembly of poly(4-vinylpyridine) (P4VP) and arylamine *N*-oxygenase CmlI. The resulting enzyme-hybridized particles, P4VP-CmlI, showed excellent catalytic activities on the oxidation of two arylamine substrates, i.e., *p*-aminophenol (*p*AP) and *p*-aminobenzoic acid (*p*ABA), using a surrogate redox system or a peroxide shunt as co-oxidants. In comparison with the free enzyme, P4VP-CmlI particles exhibited a significantly enhanced catalytic efficiency when using pyridine nucleotide (NADH) and proper redox mediators. Products at different oxygenation stages were observed. On the contrary, the activity of the enzyme-containing nanoparticles was very similar to the free enzyme when using the peroxide shunt. The enhanced catalytic efficiency of the P4VP-CmlI assemblies is attributed to a more efficient electron delivery.

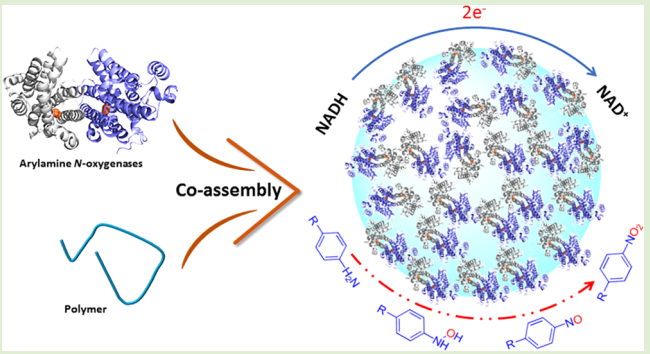

INTRODUCTION

Nitro- and nitrosoaromatic compounds[1,2] are two important classes of chemicals that have been widely used as pharmaceuticals, pesticides, dyes, explosives, and building blocks for synthesis and materials development.[3−7] Although various synthetic methods have been developed over the decades,[1,2,8] safety concerns, a lack of regioselectivity, and the resulting instability of the nitroso compounds under the harsh preparatory conditions often limit their preparation. As with other transformations, biocatalytic platforms that can be carried out under mild reaction conditions have attracted significant attention for synthetic applications for these compounds.[9−11]

Arylamine *N*-oxygenases catalyze the six-electron oxidation of aryl-amines to aryl-nitro compounds via hydroxylamine and nitroso intermediates,[12−16] providing a novel tool for stepwise synthesis of nitro- and nitrosoaromatic compounds. Among these newly characterized enzymes, CmlI is a representative arylamine *N*-oxygenase that utilizes a dinuclear-iron cofactor to catalyze the formation of the bioactive nitro group of the antibiotic chloramphenicol (CAM) via oxidation of the arylamine precursor (NH_2−CAM).[16] The mechanism and structure of CmlI reveal that the enzyme catalyzes *N*-oxygenation through successive reactions with an atypical (relative to other dinuclear oxygenases) and highly stable peroxo-diferric intermediate that is generated from reaction of the reduced diferrous protein with dioxygen.[17−19] Interestingly, in addition to the final nitro-containing compound, nitroso products can also accumulate in the enzymatic reaction with native substrate, NH_2−CAM.[17] Thus CmlI may be a promising biocatalyst for leveraging the synthesis of nitro- and nitrosoaromatic compounds if the oxygenation process can be controlled.

The use of *N*-oxygenases such as CmlI for synthetic applications is restricted by low catalytic efficiency. A native redox partner system that generates the diferrous form that subsequently reacts with O_2 has yet to be identified. It has been reported that the activity of CmlI, and AurF, a closely related ortholog involved in aureothin biosynthesis, can be reconstituted using a surrogate redox system composed of reduced pyridine nucleotide (NADH) and the redox-mediator phenazine methosulfate (PMS) (Scheme 1).[16,20] However, the uncoupled consumption of reducing equivalents likely results in the generation of damaging reactive oxygen species that may limit activity. An alternative method is to use H_2O_2 to bypass the need for reducing equivalents altogether and generate the reactive peroxo species directly (Scheme 1). This approach has been used to initiate turnover in various dinuclear-iron enzymes (e.g., AurF, soluble methane monooxygenase (sMMO), and toluene 4-monooxygenase (T4Mo)),[21−24] and variable levels of enzyme activity have been reported. For example, recent studies that have explored the shunt pathway in CmlI have shown that the addition of H_2O_2 to the diferric enzyme does not readily form the reactive peroxo-adduct that reacts with substrates.[18]

Received: December 6, 2017
Revised: January 29, 2018
Published: February 20, 2018

DOI: 10.1021/acs.biomac.7b01706
Biomacromolecules XXXX, XXX, XXX−XXX

Scheme 1. Illustration of the Reconstitution of CmlI Activity Using NADH/PMS and Dioxygen or via a Peroxide Shunt To Generate a Diferric-Peroxide Intermediate That Reacts with Arylamine Substrates[a]

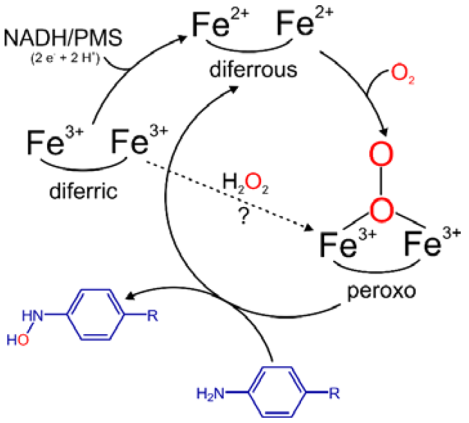

[a]Reaction regenerates the diferrous form that can further oxidize the hydroxylamine product.

Polymer–enzyme hybrids have served as an alternative method for enzyme engineering. Upon polymer conjugation, many enzymes can exhibit improved stability, pH, or temperature tolerance and catalytic efficiency with different mechanisms imparted by specific polymer structures.[25−30] The construction and characterization of pyridine-grafted polymer–protein core–shell nanoparticles (PPCS-NPs) has been systematically discussed in previous studies by our laboratory.[31−36] The synthesis of PPCS-NPs is primarily entropically driven, while the resultant nanoparticles are stabilized by synergistic interactions between polymers and proteins. The finely balanced microenvironment can help to preserve enzyme conformation and function.[36] With a robust one-step coassembly protocol, the percentage of proteins bound on the surface of the PPCS-NPs was >90% in comparison with the initial amount of the protein used. The PPCS-NPs were found to be typically stable in solution for about 1 to 2 weeks at room temperature and 4 weeks at 4 °C. During the process, no protein leaching has been observed.[36] A broad range of functional proteins and protein cages has been reported to coassemble with specific polymers to form PPCS-NPs.[36−38] Moreover, the pyridine-containing polymers can exhibit a high electron affinity and favorable electron-donation properties from the pyridine unit.[39−41] Collectively, these studies indicate that P4VP polymer assembly may be leveraged with CmlI to improve its performance as a biocatalyst. In the present study, we have generated P4VP-CmlI core–shell nanoparticles through a coassembly process and tested their catalytic activity with the arylamine substrates *p*AP and *p*ABA. Interestingly, we observed that different intermediate products accumulate with these two substrates. We found that P4VP-CmlI showed significantly higher activity on both substrates than the free enzyme that is attributed to a more efficient electron delivery process due to proximity of enzymes and cofactors. This step is rate-limiting in many classes of oxidoreductases,[42,43] and the identification of native redox-delivery systems can be a major bottleneck if the genes that encode them are located outside of the immediate genetic locus. As a result, the P4VP–enzyme assembly method may be generally applicable to leverage oxidoreductase catalysis in a variety of synthetic platforms.

EXPERIMENTAL SECTION

Materials. P4VP (M_w 60 000), *p*-aminophenol (*p*AP, >99.0%), flavin mononucleotide (FMN), and riboflavin were purchased from Sigma-Aldrich. Phenazine methosulfate (PMS, > 98.0%) and *p*-aminobenzoate (*p*ABA, >99.0%) were purchased from TCI America. NADH sodium salt was purchased from EMD Millipore. Unless otherwise noted, all chemicals and solvents used were of analytical grade and were used as received from commercial sources. Water (18.2 MΩ) was obtained from Milli-Q system (Millipore). Unless otherwise noted, all buffers are 50 mM 3-(*N*-morpholino) propane sulfonic acid (MOPS), pH 7.4.

Heterologous Expression and Purification of CmlI. The *Streptomyces venezuelae* CmlI gene, cloned into the pVP91A expression vector and characterized in previous studies,[19] was used for protein expression. This vector contains an eight-histidine tag at the *N*-terminus to facilitate purification. Expression of CmlI was performed in *E. coli* BL21 (DE3) in LB medium in the presence of 100 μg/mL ampicillin. Cells were grown to an OD ∼1.0 and induced with 150 μM IPTG and 50 μM $FeCl_3$, at which point the temperature was lowered to 20 °C, and grown for an additional 15 h. Cells were harvested by centrifugation for purification or stored at −80 °C for further use. The protein was purified using nickel–nitriloacetic acid (Ni–NTA) affinity chromatography as described previously[19] and was subsequently dialyzed against 50 mM MOPS pH 7.4 buffer and stored at −80 °C until further use. Enzyme purity was assessed by SDS-PAGE, and the iron-to-enzyme ratio was verified by the ferrozine assay (Figure S1).[44]

Synthesis of P4VP-CmlI Assemblies. A solution of P4VP in ethanol (7.5 mg·mL^{-1}, 0.1 mL) was slowly added to a solution containing CmlI in 50 mM MOPS pH 7.4 (1.2 mg·mL^{-1}, 0.9 mL) with stirring. After addition, the mixture was stirred for an additional 30 min. To study the influence of FMN reduction by NADH, the P4VP-CmlI assemblies were prepared with a similar procedure but with diluted P4VP (0.75 mg·mL^{-1}, 0.1 mL) and CmlI enzyme (0.12 mg·mL^{-1}, 0.9 mL) in 50 mM MOPS pH 7.4. All of the assembled samples were freshly prepared in the characterization and activity test.

Characterization of P4VP-CmlI Assemblies. The P4VP-CmlI sample (20 μL) was centrifuged to collect the nanoparticles and resuspended with the same volume of water, dropped onto a stub, and dried in the hood, then coated with a thin layer of gold film using a Denton Vacuum Desk II. The sputtered samples were fixed onto the sample holder and placed in the vacuum chamber of the microscope under low vacuum (1025 Torr) for imaging by the in-lens detector of Zeiss Ultraplus thermal field-emission scanning electron microscope (FESEM). For TEM analysis, the sample was diluted 100 times by water, and 20 μL of diluted sample was dropped onto 300-mesh carbon-coated copper grids and dried. The grids were then stained with 20 μL of uranyl acetate (2% w/v) for 5 min and observed with a Hitachi H-8000 electron microscope. The size distribution of P4VP-CmlI assemblies was measured with dynamic light scattering (DLS, Zetasizer Nano ZS, Malvern Instruments). The mean value for the size based on the intensity and the polydispersity index (PDI), a dimensionless width parameter based on the cumulant analysis, were detected.

Activity Assay of P4VP-CmlI Assemblies and Free CmlI. The activity assay of both P4VP-CmlI and free CmlI was performed in a reaction volume of 100 μL. The final reaction mixture contained CmlI (20 μM), the substrate *p*AP or *p*ABA (1 mM), PMS or FMN or riboflavin (12.5–125 μM), NADH (1–10 mM), and 7% ethanol in MOPS buffer. Reactions were performed at room temperature (23–25 °C) and were initiated by the addition of the substrate to the reaction mixture. The specific activity was calculated during the first 10 min. The PMS, FMN, and riboflavin reagent were freshly prepared and kept in the dark until use. NADH and PMS or FMN or riboflavin were added immediately before each reaction to minimize any possible side reactions in the presence of oxygen.[45] P4VP-CmlI and CmlI reactions were prepared and tested side-by-side for an accurate comparison of activity. Reactions with *p*AP were measured by monitoring *p*NOP product formation at an absorbance of 405 nm with a Molecular Device SPECTRAMax plus 384 with a microplate reader using 0.33

DOI: 10.1021/acs.biomac.7b01706
Biomacromolecules XXXX, XXX, XXX–XXX

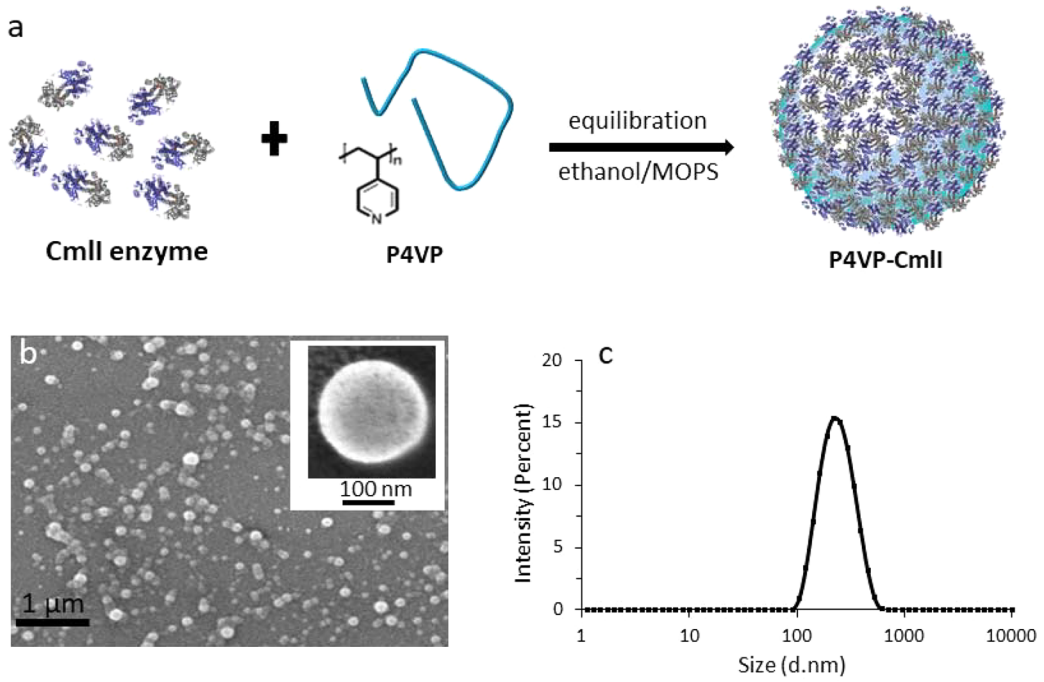

Figure 1. (a) Schematic representation of the preparation of P4VP-CmlI in MOPS buffer at pH 7.4. (b) FESEM image of P4VP-CmlI nanoparticles. Inset shows an enlarged image of a single particle. (c) Size distribution of P4VP-CmlI nanoparticles based on DLS measurement.

Scheme 2. Schematic Representation of CmlI-Catalyzed Reaction with *p*AP and *p*ABA as Substrate, Respectively

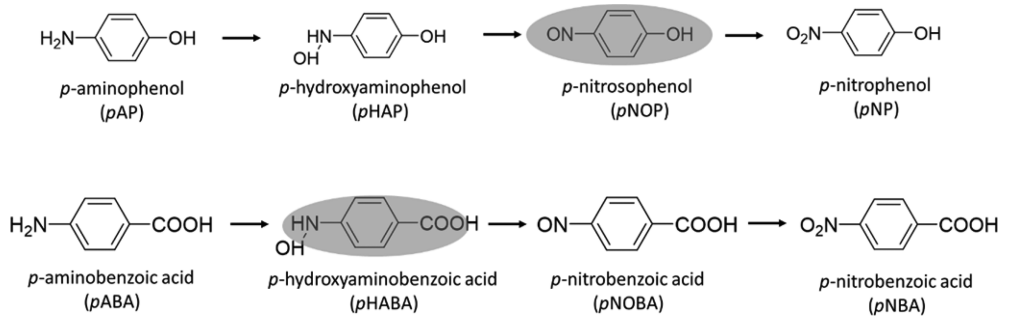

[a]Shaded products were observed with NADH/PMS method.

cm path length. The activity assay with *p*ABA was performed with the same procedure, and the products were quantified by HPLC as described below. The assays were performed in at least triplicate and the averages were reported.

Peroxide-Shunt Assay. Peroxide-shunt experiments were performed by the addition of H_2O_2 to the solution containing enzyme and substrate. Final reactions contained CmlI (20 μM), *p*AP or *p*ABA (1 mM), 1.5% H_2O_2 (v/v) and 7% ethanol in MOPS buffer (50 mM, pH 7.4). The activity was quantified by HPLC as described below. To compare the stability and activity of the assembled enzyme complexes with that of the free enzyme, a pretreatment time course study was done with preincubation of P4VP-CmlI and free enzymes with 1.5% H_2O_2 (v/v) for 0, 1, 2, and 5 h; then, the activity test was followed.

HPLC and MS Analysis. Reactions with *p*AP were quenched by trifluoroacetic acid (final concentration 2.5% v/v). Reactions with *p*ABA were quenched using acetic acid (final concentration 1% v/v). After quenching, samples were centrifuged at 14 000 rpm at 4 °C for 15 min and the supernatant was collected. Because of the sensitivity of aryl-nitroso compounds toward NADH,[46] both P4VP-CmlI and free CmlI-catalyzed reactions were analyzed by HPLC immediately after quenching and centrifugation. The products were identified and quantified using an Agilent 1100 series HPLC equipped with a ZORBAX SB-C18 column. HPLC parameters were as follows: 25 °C; solvent A, 1% acetic acid in water; solvent B, methanol; gradient, 10% B for 2 min; then, from 10% B to 100% B over 18 min; flow rate, 0.5 mL/min. Detection of the products resulting from *p*AP metabolism was done by UV absorbance at 305 nm. Those from *p*ABA reactions were monitored at 268 nm. Quantification was done based on the peak area of the corresponding compounds. LC−MS with electrospray ionization was carried out in Mass Spectrometry Center, USC to identify the *p*HABA.

FMN Reduction Rate Test. 50 mM MOPS pH 7.4 buffer was degassed for 30 min before it was used for P4VP-CmlI assembly, and solutions of FMN (500 μM), NADH (50 mM), and P4VP- and free CmlI enzyme were degassed separately for 10 min and diluted with MOPS buffer before each test. UV−vis absorption studies were performed using an Agilent 8453 UV−vis spectrometer (1 mm path length) with exposure to air.

RESULTS AND DISCUSSION

P4VP-CmlI Synthesis and Characterization. A robust one-step protocol for PPCS-NPs generation through coassembly was described in detail in previous studies.[36] In brief, P4VP polymer was dissolved in ethanol then added dropwise to CmlI enzyme solution with vigorous stirring. After addition, the mixture was stirred for an additional 30 min for equilibration

DOI: 10.1021/acs.biomac.7b01706
Biomacromolecules XXXX, XXX, XXX−XXX

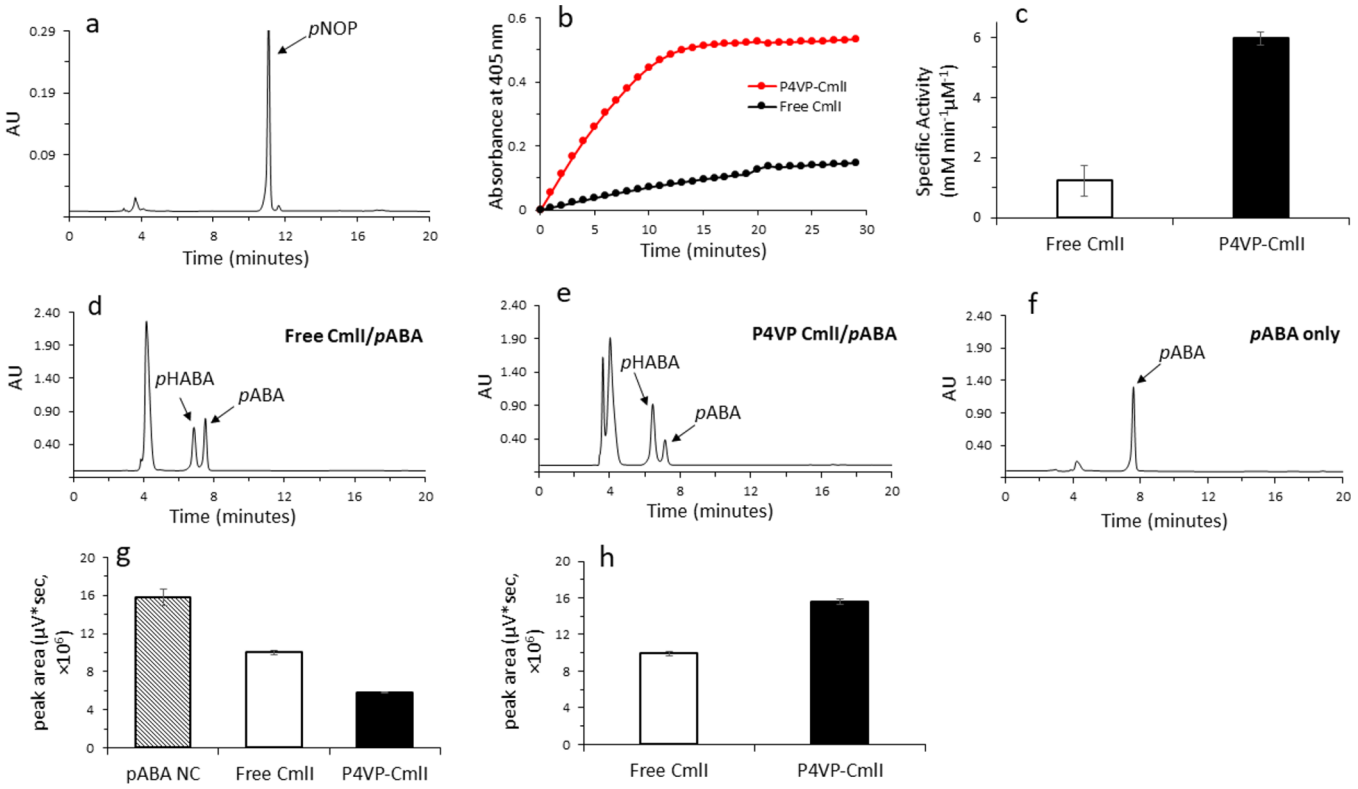

Figure 2. Enzymatic activity analysis of P4VP-CmlI assemblies: 20 μM enzyme, 1 mM *p*AP or 1 mM *p*ABA, 2 mM NADH and 25 μM PMS in MOPS buffer (50 mM, pH 7.4). (a) HPLC analysis of the enzymatic oxidation products of *p*AP catalyzed with P4VP-CmlI. (b,c) Comparison of the activity of P4VP-CmlI and free CmlI using *p*AP-based chromogenic assay; the signal at the first read was subtracted as background. HPLC analysis of the oxidation products using *p*ABA as the substrate with (d) free CmlI and (e) P4VP-CmlI as the catalyst and (f) the pure *p*ABA. (g,h) Activity comparison based on the consumption of starting material *p*ABA (g) and the production of the intermediate *p*HABA (h). Error bars represent the standard deviation of the mean of triplicate samples.

(Figure 1a). Because of the high loading capacity of the PPCS-NPs,[36] in this work the equilibrated P4VP-CmlI sample was used in the morphology test and enzymatic assay without a further purification. On the basis of the FESEM (Figure 1b) and TEM (Figure S2), P4VP-CmlI core−shell nanoparticles could be successfully generated. On the basis of DLS analysis, the average diameter of P4VP-CmlI nanoparticles was ∼200 nm and the PDI was 0.107, showing considerable homogeneous nanoparticles formed (Figure 1c). This was consistent with our previous research results.[32,36]

Catalytic Activity Analysis of P4VP-CmlI. Aside from reactions with the native NH_2−CAM substrate, there is only limited data that define the substrate scope for CmlI reactions.[16] From transient kinetics measurements, it is known that the peroxo-CmlI adduct exhibits enhanced rates of decay in the presence of arylamine compounds with different para substituents including *p*AP, *p*ABA, and L-*p*APA (L-*para*-aminophenylalanine).[19] However, the products for these reactions have not been identified. In this study, *p*AP and *p*ABA were chosen as model substrates for characterizing P4VP-CmlI activity. On the basis of reported catalytic mechanism of CmlI, the nitro substituted compounds (*p*NP and *p*NBA) should be produced as the final six-electron oxidized products, while the analogous hydroxylamino (*p*HAP and *p*HABA) and nitroso compounds (*p*NOP and *p*NOBA) may be observed as intermediate products (Scheme 2).[17] It was reported that PsAAO, a closely related ortholog of AurF and CmlI, could tolerate and even showed higher activity in the presence of methanol.[21] We found that CmlI had similar characteristics; that is, the presence of 7% ethanol increased the enzyme activity by ∼50% (data not shown). As a result, the P4VP-CmlI NPs were tested in the 7% ethanol/MOPS cosolvent without further purification after the coassembly.

The activity of P4VP-CmlI was reconstituted using a redox system composed of NADH and the mediator PMS. The activity was alternatively assessed with a peroxide-shunt method using 1.5% H_2O_2 (v/v). The *p*AP and *p*ABA substrates tested here have opposing electrophilicities at the para substitution (Scheme 2). Very interestingly, while both *p*AP and *p*ABA could serve as substrates for CmlI, we observed that for *p*AP, the intermediate product *p*NOP rather than the fully oxidized *p*NP was accumulated for both the P4VP-CmlI- and free CmlI-catalyzed reactions using either method (Figure 2a, Figure S4). In contrast, when *p*ABA was used as a substrate, the intermediate product *p*HABA was accumulated with the NADH/PMS method (Figure 2d−f) and *p*NBA was detected with the peroxide-shunt method (Figure S6). For comparison, the ortholog AurF was reported to have activity with *p*ABA, but no activity was observed with *p*AP.[22] AurF also exhibits product distributions that depend on the turnover methods utilized, which was attributed to different reaction steps being rate-limiting.[22]

The mechanisms why intermediate products can escape from the enzyme active center have not been well understood so far. In this study, it could be attributed to the smaller size of the two unnatural substrates relative to their native counterpart, NH_2−CAM, which may enable them to be released from the enzyme active center prior to complete oxidation. The

DOI: 10.1021/acs.biomac.7b01706
Biomacromolecules XXXX, XXX, XXX−XXX

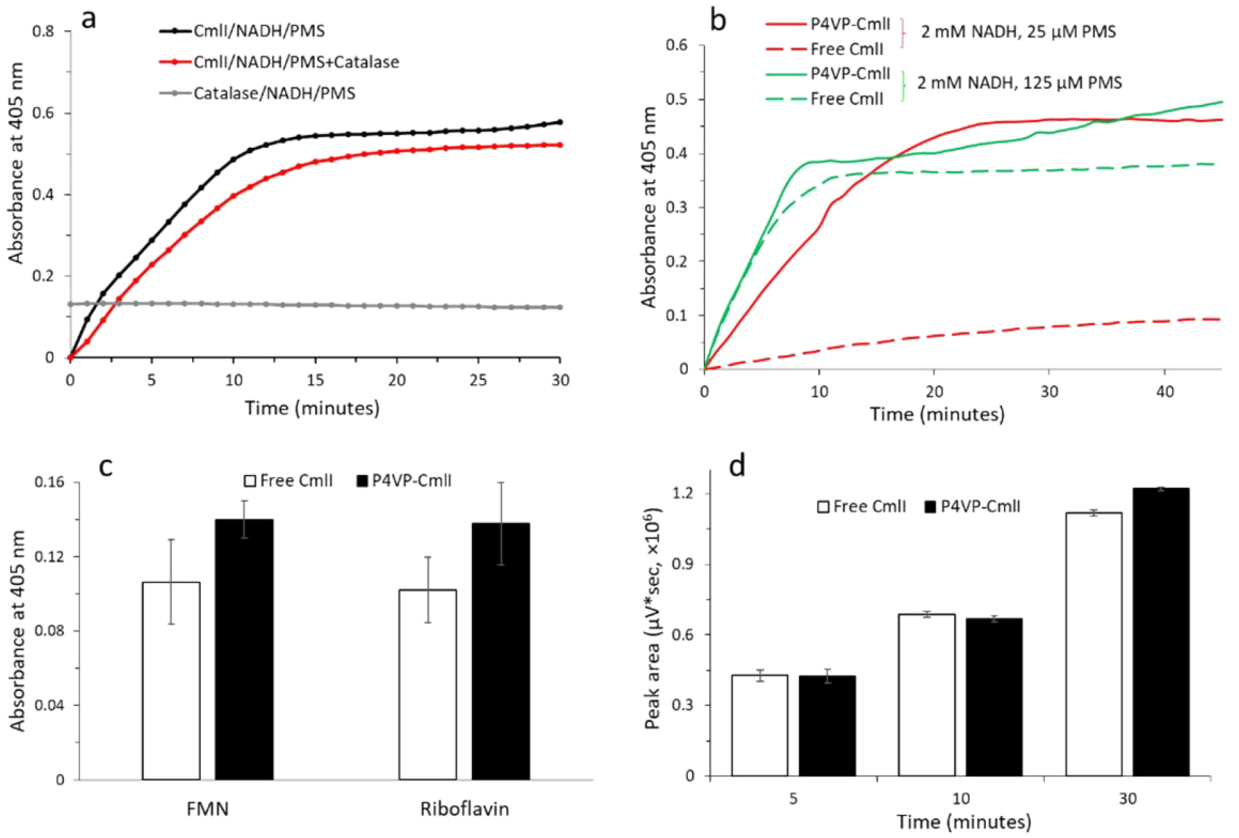

Figure 3. Enzymatic activity comparison of P4VP-CmlI and free CmlI with addition of catalase (a), with different PMS/NADH concentration (b), with NADH/FMN or NADH/riboflavin system (c), and by peroxo-shunt method (d). For panel a, 25 μM CmlI was used in CmlI/NADH/PMS reaction and 25 μM CmlI and 1 μM catalase were used in CmlI/NADH/PMS + catalase reaction. All reactions were done with 2.5 mM NADH, 125 μM PMS, 1 mM *p*AP, 7% ethanol in MOPS buffer (50 mM, pH 7.4). For panel c, 1 mM NADH and 12.5 μM FMN or riboflavin was used and the reaction was stopped at 60 min. For panel d, 1.5% H_2O_2 (v/v) was used. From panels b to d, the reactions were done with 20 μM enzyme, 1 mM *p*AP in MOPS buffer (50 mM, pH 7.4). Error bars represent the standard deviation of the mean of triplicate tests.

proposed mechanism for CmlI catalysis invokes an ambiphilic nature of the peroxo-CmlI oxidant, which could perform electrophilic (for amine or hydroxylamino) or nucleophilic oxidations (for nitroso) substrates, respectively.[17] Each of these would be expected to be highly sensitive to the nature of the para substituent. As a result, product distributions and activity would be expected to alter as we observed here.

With P4VP assembly, enzyme functionality was maintained. It is noteworthy that the activity of enzyme assembly with NADH/PMS method showed around 1.6 to 2.3 times increase compared with the activity carried out via the peroxide shunt method. In addition, the enzyme activity results showed near-ideal enzyme activity behavior, especially in the early time regime. For longer reaction time, it showed a biphasic behavior. As a result of this more complex process, kinetics rates are not calculated in this work. We still do not know the precise origins for such phenomenon. However, a similar observation has been also reported by another group.[16] To the best of our knowledge, this study is the first report that, with different substrates, products at different oxygenation stages can be selectively enriched by CmlI. Continued investigation using a wider substrate-scope may reveal new opportunities for synthetic applications.

Activity Comparison of P4VP-CmlI and Free CmlI. To compare the catalytic efficiency of P4VP-CmlI and free CmlI, the free enzyme was tested under the same conditions used in the preparation of P4VP-CmlI. For *p*AP with NADH/PMS method, reactions were monitored by absorbance spectroscopy (λ = 405 nm) to monitor the production of *p*NOP (Figure 2b). The specific activity of P4VP-CmlI was as much as five times higher than that of the free enzyme (Figure 2c). For *p*ABA, the activity of P4VP-CmlI was ~1.6 times that of free enzyme, as calculated by either the consumption of substrate (Figure 2g) or by *p*HABA production (Figure 2h) through the HPLC quantification.

The reaction of PMS and NADH has been reported to produce hydrogen peroxide,[47] which at high enough levels may contribute to enzyme activity. To test this possibility, 1 μM catalase was included in the CmlI/*p*AP/NADH/PMS reaction. Only minor differences in activity were observed upon the addition of the H_2O_2 scavenger (Figure 3a). This suggests that CmlI catalysis from pyridine nucleotide likely proceeds by a reductive mechanism where the peroxo-adduct is formed from electron transfer and subsequent O_2 binding. Under the turnover conditions employed in this study and the rates of turnover we measured, it is unlikely that superoxide has a sufficient lifetime to support reactions prior to its decomposition to hydrogen peroxide. Importantly, superoxide is unlikely to generate the relevant peroxo-intermediate (from the diferric resting state), which has been shown to be the reactive species in CmlI (and by extension AurF) catalysis in previous studies because it does not provide the two reducing equivalents necessary.

DOI: 10.1021/acs.biomac.7b01706
Biomacromolecules XXXX, XXX, XXX−XXX

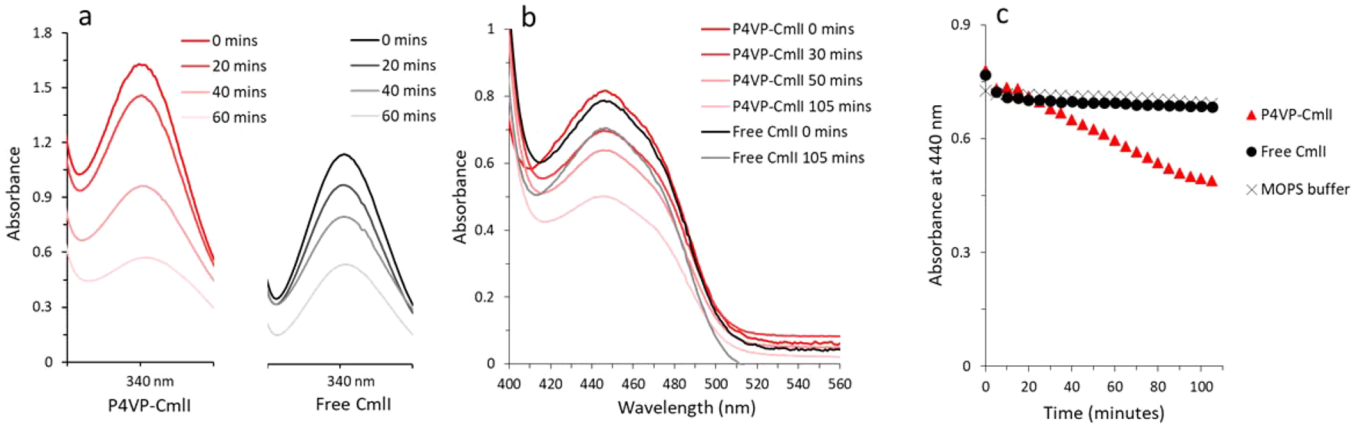

Figure 4. Reduction test of FMN by NADH in P4VP-CmlI and free CmlI solution. (a) UV−vis spectra of P4VP-CmlI solution (red) and free CmlI solution (black) at MOPS buffer. (b) Time-resolved NADH signal (200 μM) in the presence of FMN (30 μM) in P4VP-CmlI and free CmlI solution. (c) Time courses for the reduction of FMN (50 μM) by NADH (5 mM) in P4VP-CmlI solution, free CmlI solution, and MOPS buffer.

To further explore why P4VP-CmlI exhibits enhanced turnover, the enzymatic activity assay with *p*AP was performed at different NADH/PMS concentrations. As expected, when both NADH and PMS were at higher concentrations (NADH 10 mM, PMS 125 μM), both P4VP-CmlI and free CmlI showed higher activity due to faster electron delivery (Figure S3). However, when the concentration of PMS was increased from 125 μM but the NADH was kept at 2 mM, the difference between the activities of P4VP-CmlI and free CmlI became negligible due to the dramatically increased turnover of the free enzyme (Figure 3b). This implies that the electron-transferring process mediated by PMS could be facilitated in the P4VP-CmlI reaction, and this difference was masked by increasing PMS concentration. It is noteworthy that product formation time course by CmlI showed a lag-phase, possibly due to a side reaction between the nitroso intermediate and NADH/PMS.[46] Interestingly, this effect can be rescued in the P4VP-CmlI catalyzed reaction (Figure S3). This phenomenon could be attributed to potential interactions between P4VP polymer scaffold and PMS, which is still under investigation.

FMN and riboflavin, common biological redox partners used in a plethora of redox processes,[48−50] were utilized as an alternative reducing system. As shown in Figure 3c and consistent with the results from PMS, the activity of P4VP-CmlI was higher (~30%) than the free enzyme with *p*AP substrate. However, the overall efficiency was much lower than that of the NADH/PMS couple.

On the basis of above data, we hypothesized that the origin of the enhanced activity for P4VP-CmlI may derive from an enhanced rate of electron delivery to form the diferrous cluster. To test this, the activity of P4VP-CmlI and free CmlI was compared to a peroxide-shunt method in which the reduction process was bypassed (Scheme 1). The result showed no significant activity difference between the P4VP-CmlI and free CmlI (Figure 3d). This indicated that the enhanced activity of P4VP using NADH was most likely from the enzyme reduction step. To further identify the effect of H_2O_2 on the stability and activity of peroxo CmlI intermediate under assembled and free conditions, the H_2O_2 pretreatment study was performed. In this test, both P4VP-CmlI and free CmlI were pretreated with 1.5% H_2O_2 (v/v) and aged for different times prior to the addition of *p*AP. There was no significant difference between P4VP-CmlI and CmlI, indicating uncompromised stability and activity of both samples (Figure S5).

FMN Reduction Test in P4VP-CmlI and Free CmlI Solutions. To further demonstrate that an enhancement in electron transfer conferred higher activity in P4VP-CmlI, the transfer of electrons from NADH to FMN was tested by optical spectroscopy. NADH, in its reduced form, absorbs at 340 nm and FMN, in its oxidized form, absorbs at 440 nm. The reduction of FMN by NADH can thus be monitored by the loss of absorbance at both wavelengths. The absorbance spectrum of P4VP-CmlI has background contributions due to scattering of the nanoparticles (Figure S7). As one could expect, oxidation of NADH occurs for both P4VP-CmlI and free CmlI due to the reaction of FMN and NADH. However, P4VP-CmlI shows a much faster rate of NADH oxidation (Figure 4a) and as a consequence significantly faster FMN reduction (Figure 4b,c).

CONCLUSIONS

We have generated P4VP-CmlI core−shell nanoparticles via a facile self-assembly process and explored its activity with two substrates *p*AP and *p*ABA using both oxidative and reductive turnover methods. Nitroso and nitro products could be selectively produced with different substrates using different cosubstrates to initiate the reaction. We found that the P4VP assembly could significantly increase CmlI activity using NADH as an electron source and appropriate electron mediators. Because redox partners are required for the efficient turnover of CmlI but have yet to be identified, reconstitution of the enzyme activity in vitro is a major challenge. The P4VP polymer assembly system improves the reduction of the enzyme in the absence of protein-based redox partners and as a result shows significant enhanced activity. P4VP is an inexpensive polymer available on an industrial scale, and the polymer−enzyme coassembly process is both robust and facile. The P4VP-CmlI nanoparticles reported here could thus be easily used for synthetic applications. Further investigations on a broad range of substrates of P4VP-CmlI and an expansion of this strategy to other oxidoreductases are currently underway in our laboratories.

DOI: 10.1021/acs.biomac.7b01706
Biomacromolecules XXXX, XXX, XXX−XXX

■ ASSOCIATED CONTENT

Supporting Information

The Supporting Information is available free of charge on the ACS Publications website at DOI: 10.1021/acs.biomac.7b01706.

Figure S1. SDS-PAGE and iron content identification of CmlI enzyme by ferrozine assay. Figure S2. TEM image of P4VP-CmlI nanoparticles. Figure S3. Enzymatic activity comparison of P4VP-CmlI and free CmlI with NADH 10 mM, PMS 125 μM. Figure S4. HPLC result of P4VP-CmlI assembly and free CmlI enzyme reaction with pAP with different assays including the reactions with 2 mM NADH, 125 μM PMS, the reactions with 1.5% H_2O_2, P4VP-CmlI-catalyzed reaction with NADH/FMN, P4VP-CmlI-catalyzed reaction with NADH/riboflavin, HPLC traces of pNOP and pNP standards. Figure S5. P4VP-CmlI and free CmlI activity test with different time of H_2O_2 pretreatment using pAP as substrate. Figure S6. P4VP-CmlI and free CmlI activity test with H_2O_2 method using pABA as substrate. Figure S7. UV−vis spectra of P4VP-CmlI solution and free CmlI solution at MOPS buffer. Figure S8. HPLC traces of pNBA standard and the identification of pHABA produced in the P4VP-CmlI with NADH/PMS method by LC−MS.(PDF)

■ AUTHOR INFORMATION

Corresponding Authors

*T.M.M.: E-mail: makrist@mailbox.sc.edu.
*Q.W.: E-mail: wang263@mailbox.sc.edu.

ORCID

Thomas M. Makris: 0000-0001-7927-620X
Qian Wang: 0000-0002-2149-384X

Notes

The authors declare no competing financial interest.

■ ACKNOWLEDGMENTS

This material is based on work supported by the National Science Foundation under grant no. OIA-1655740 and an ASPIRE grant from the University of South Carolina. We thank Lin Lv, Panita Maturavongsadit, Dr. Kamolrat Metavarayuth, and Dr. Jibin Zhao for the assistance with coassembly and EM analysis and their helpful comments and discussion.

■ REFERENCES

(1) Ju, K.-S.; Parales, R. E. Nitroaromatic Compounds, from Synthesis to Biodegradation. *Microbiol. Mol. Biol. Rev. MMBR* **2010**, *74*, 250−272.
(2) Gowenlock, B. G.; Richter-Addo, G. B. Preparations of C-Nitroso Compounds. *Chem. Rev.* **2004**, *104*, 3315−3340.
(3) Strauss, M. J. The Nitroaromatic Group in Drug Design. Pharmacology and Toxicology (for Nonpharmacologists). *Ind. Eng. Chem. Prod. Res. Dev.* **1979**, *18*, 158−166.
(4) Shanmugaraju, S.; Joshi, S. A.; Mukherjee, P. S. Fluorescence and Visual Sensing of Nitroaromatic Explosives Using Electron Rich Discrete Fluorophores. *J. Mater. Chem.* **2011**, *21*, 9130−9138.
(5) Fan, F.-R. F.; Yao, Y.; Cai, L.; Cheng, L.; Tour, J. M.; Bard, A. J. Structure-Dependent Charge Transport and Storage in Self-Assembled Monolayers of Compounds of Interest in Molecular Electronics: Effects of Tip Material, Headgroup, and Surface Concentration. *J. Am. Chem. Soc.* **2004**, *126*, 4035−4042.
(6) Ranganathan, D.; Rao, C. B.; Ranganathan, S.; Mehrotra, A. K.; Iyengar, R. Nitroethylene: A Stable, Clean, and Reactive Agent for Organic Synthesis. *J. Org. Chem.* **1980**, *45*, 1185−1189.
(7) King, S. B.C-Nitroso Compounds, Oximes, N-Hydroxyguanidines and N-Hydroxyureas. In *Nitric Oxide Donors*; Wang, P. G., Cai, T. B., Taniguchi, N., Eds.; Wiley-VCH: Weinheim, Germany, 2005; pp 177−199.
(8) Yan, G.; Yang, M. Recent Advances in the Synthesis of Aromatic Nitro Compounds. *Org. Biomol. Chem.* **2013**, *11*, 2554−2566.
(9) Schmid, A.; Dordick, J. S.; Hauer, B.; Kiener, A.; Wubbolts, M.; Witholt, B. Industrial Biocatalysis Today and Tomorrow. *Nature* **2001**, *409*, 258−268.
(10) Choi, J.-M.; Han, S.-S.; Kim, H.-S. Industrial Applications of Enzyme Biocatalysis: Current Status and Future Aspects. *Biotechnol. Adv.* **2015**, *33*, 1443−1454.
(11) Winkler, R.; Hertweck, C. Biosynthesis of Nitro Compounds. *ChemBioChem* **2007**, *8*, 973−977.
(12) Lee, J.; Simurdiak, M.; Zhao, H. Reconstitution and Characterization of Aminopyrrolnitrin Oxygenase, a Rieske N-Oxygenase That Catalyzes Unusual Arylamine Oxidation. *J. Biol. Chem.* **2005**, *280*, 36719−36727.
(13) He, J.; Hertweck, C. Biosynthetic Origin of the Rare Nitroaryl Moiety of the Polyketide Antibiotic Aureothin: Involvement of an Unprecedented N-Oxygenase. *J. Am. Chem. Soc.* **2004**, *126*, 3694−3695.
(14) Simurdiak, M.; Lee, J.; Zhao, H. A New Class of Arylamine Oxygenases: Evidence That p-Aminobenzoate N-Oxygenase (AurF) Is a Di-Iron Enzyme and Further Mechanistic Studies. *ChemBioChem* **2006**, *7*, 1169−1172.
(15) Li, N.; Korboukh, V. K.; Krebs, C.; Bollinger, J. M. Four-Electron Oxidation of p-Hydroxylaminobenzoate to p-Nitrobenzoate by a Peroxodiferric Complex in AurF from Streptomyces Thioluteus. *Proc. Natl. Acad. Sci. U. S. A.* **2010**, *107*, 15722−15727.
(16) Lu, H.; Chanco, E.; Zhao, H. CmlI Is an N-Oxygenase in the Biosynthesis of Chloramphenicol. *Tetrahedron* **2012**, *68*, 7651.
(17) Komor, A. J.; Rivard, B. S.; Fan, R.; Guo, Y.; Que, L.; Lipscomb, J. D. Mechanism for Six-Electron Aryl-N-Oxygenation by the Non-Heme Diiron Enzyme CmlI. *J. Am. Chem. Soc.* **2016**, *138*, 7411−7421.
(18) Knoot, C. J.; Kovaleva, E. G.; Lipscomb, J. D. Crystal Structure of CmlI, the Arylamine Oxygenase from the Chloramphenicol Biosynthetic Pathway. *JBIC, J. Biol. Inorg. Chem.* **2016**, *21*, 589−603.
(19) Makris, T. M.; Vu, V. V.; Meier, K. K.; Komor, A. J.; Rivard, B. S.; Münck, E.; Que, L.; Lipscomb, J. D. An Unusual Peroxo Intermediate of the Arylamine Oxygenase of the Chloramphenicol Biosynthetic Pathway. *J. Am. Chem. Soc.* **2015**, *137*, 1608−1617.
(20) Choi, Y. S.; Zhang, H.; Brunzelle, J. S.; Nair, S. K.; Zhao, H. In Vitro Reconstitution and Crystal Structure of P-Aminobenzoate N-Oxygenase (AurF) Involved in Aureothin Biosynthesis. *Proc. Natl. Acad. Sci. U. S. A.* **2008**, *105*, 6858−6863.
(21) Platter, E.; Lawson, M.; Marsh, C.; Sazinsky, M. H. Characterization of a Non-Ribosomal Peptide Synthetase-Associated Diiron Arylamine N-Oxygenase from Pseudomonas Syringae Pv. Phaseolicola. *Arch. Biochem. Biophys.* **2011**, *508*, 39−45.
(22) Chanco, E.; Choi, Y. S.; Sun, N.; Vu, M.; Zhao, H. Characterization of the N-Oxygenase AurF from Streptomyces Thioletus. *Bioorg. Med. Chem.* **2014**, *22*, 5569−5577.
(23) Andersson, K. K.; Froland, W. A.; Lee, S.-K.; Lipscomb, J. D. Dioxygen Independent Oxygenation of Hydrocarbons by Methane Monooxygenae Hydroxylase Component. *J. Inorg. Biochem.* **1991**, *43*, 557.
(24) Bailey, L. J.; Fox, B. G. Crystallographic and Catalytic Studies of the Peroxide-Shunt Reaction in a Diiron Hydroxylase. *Biochemistry* **2009**, *48*, 8932−8939.
(25) Suthiwangcharoen, N.; Nagarajan, R. Enhancing Enzyme Stability by Construction of Polymer−Enzyme Conjugate Micelles for Decontamination of Organophosphate Agents. *Biomacromolecules* **2014**, *15*, 1142−1152.
(26) Kawamura, A.; Harada, A.; Kono, K.; Kataoka, K. Self-Assembled Nano-Bioreactor from Block Ionomers with Elevated and

DOI: 10.1021/acs.biomac.7b01706
Biomacromolecules XXXX, XXX, XXX−XXX

Stabilized Enzymatic Function. *Bioconjugate Chem.* **2007**, *18*, 1555−1559.
(27) Cummings, C.; Murata, H.; Koepsel, R.; Russell, A. J. Dramatically Increased PH and Temperature Stability of Chymotrypsin Using Dual Block Polymer-Based Protein Engineering. *Biomacromolecules* **2014**, *15*, 763−771.
(28) Lee, H.; Park, T. G. Conjugation of Trypsin by Temperature-Sensitive Polymers Containing a Carbohydrate Moiety: Thermal Modulation of Enzyme Activity. *Biotechnol. Prog.* **1998**, *14*, 508−516.
(29) Lee, E.-H.; Tsujimoto, T.; Uyama, H.; Sung, M.-H.; Kim, K.; Kuramitsu, S. Enhancement of Enzyme Activity and Stability by Poly(γ-Glutamic Acid). *Polym. J.* **2010**, *42*, 818−822.
(30) Zhang, Y.; Ge, J.; Liu, Z. Enhanced Activity of Immobilized or Chemically Modified Enzymes. *ACS Catal.* **2015**, *5*, 4503−4513.
(31) Li, T.; Niu, Z.; Emrick, T.; Russell, T. P.; Wang, Q. Core/Shell Biocomposites from the Hierarchical Assembly of Bionanoparticles and Polymer. *Small* **2008**, *4*, 1624−1629.
(32) Li, T.; Ye, B.; Niu, Z.; Thompson, P.; Seifert, S.; Lee, B.; Wang, Q. Closed-Packed Colloidal Assemblies from Icosahedral Plant Virus and Polymer. *Chem. Mater.* **2009**, *21*, 1046−1050.
(33) Li, T.; Niu, Z.; Suthiwangcharoen, N.; Li, R.; Prevelige, P. E.; Wang, Q. Polymer-Virus Core-Shell Structures Prepared via Co-Assembly and Template Synthesis Methods. *Sci. China: Chem.* **2010**, *53*, 71−77.
(34) Wu, L.; Li, T.; Blom, D.; Zhao, J.; Ghoshroy, S.; Wang, Q. Synthesis and Electron Microscopic Analysis of the Self-Assembly of Polymer and Ferritin Core-Shell Structures. *Microsc. Res. Tech.* **2011**, *74*, 636−641.
(35) Li, T.; Wu, L.; Suthiwangcharoen, N.; Bruckman, M. A.; Cash, D.; Hudson, J. S.; Ghoshroy, S.; Wang, Q. Controlled assembly of rodlike viruses with polymers. *Chem. Commun.* **2009**, 2869−2871.
(36) Suthiwangcharoen, N.; Li, T.; Wu, L.; Reno, H. B.; Thompson, P.; Wang, Q. Facile Co-Assembly Process to Generate Core−Shell Nanoparticles with Functional Protein Corona. *Biomacromolecules* **2014**, *15*, 948−956.
(37) Lu, L.; Yuan, L.; Yan, J.; Tang, C.; Wang, Q. Development of Core−Shell Nanostructures by In Situ Assembly of Pyridine-Grafted Diblock Copolymer and Transferrin for Drug Delivery Applications. *Biomacromolecules* **2016**, *17*, 2321−2328.
(38) Zhang, X.; Zhao, X.; Luckanagul, J. A.; Yan, J.; Nie, Y.; Lee, L. A.; Wang, Q. Polymer−Protein Core−Shell Nanoparticles for Enhanced Antigen Immunogenicity. *ACS Macro Lett.* **2017**, *6*, 442−446.
(39) Lu, H.-F.; Chan, H. S. O.; Ng, S.-C. Synthesis, Characterization, and Electronic and Optical Properties of Donor−Acceptor Conjugated Polymers Based on Alternating Bis(3-Alkylthiophene) and Pyridine Moieties. *Macromolecules* **2003**, *36*, 1543−1552.
(40) Rochat, S.; Swager, T. M. Water-Soluble Cationic Conjugated Polymers: Response to Electron-Rich Bioanalytes. *J. Am. Chem. Soc.* **2013**, *135*, 17703−17706.
(41) Willner, I.; Riklin, A.; Lapidot, N. Electron-Transfer Communication between a Redox Polymer Matrix and an Immobilized Enzyme: Activity of Nitrate Reductase in a Viologen-Acrylamide Copolymer. *J. Am. Chem. Soc.* **1990**, *112*, 6438−6439.
(42) McMillan, D. G. G.; Marritt, S. J.; Firer-Sherwood, M. A.; Shi, L.; Richardson, D. J.; Evans, S. D.; Elliott, S. J.; Butt, J. N.; Jeuken, L. J. C. Protein−Protein Interaction Regulates the Direction of Catalysis and Electron Transfer in a Redox Enzyme Complex. *J. Am. Chem. Soc.* **2013**, *135*, 10550−10556.
(43) Suzuki, R.; Hirakawa, H.; Nagamune, T. Electron Donation to an Archaeal Cytochrome P450 Is Enhanced by PCNA-Mediated Selective Complex Formation with Foreign Redox Proteins. *Biotechnol. J.* **2014**, *9*, 1573−1581.
(44) Stookey, L. L. Ferrozine−-a New Spectrophotometric Reagent for Iron. *Anal. Chem.* **1970**, *42*, 779−781.
(45) Halaka, F. G.; Babcock, G. T.; Dye, J. L. Properties of 5-Methylphenazinium Methyl Sulfate. Reaction of the Oxidized Form with NADH and of the Reduced Form with Oxygen. *J. Biol. Chem.* **1982**, *257*, 1458−1461.
(46) Leskovac, V.; Svircević, J.; Trivić, S.; Popović, M.; Radulović, M. Reduction of Aryl-Nitroso Compounds by Pyridine and Flavin Coenzymes. *Int. J. Biochem.* **1989**, *21*, 825−834.
(47) Halliwell, B. Hydroxylation of Aromatic Compounds by Reduced Nicotinamide-Adenine Dinucleotide and Phenazine Methosulphate Requires Hydrogen Peroxide and Hydroxyl Radicals, but Not Superoxide. *Biochem. J.* **1977**, *167*, 317−320.
(48) Gutman, M. Electron Flux through the Mitochondrial Ubiquinone. *Biochim. Biophys. Acta, Rev. Bioenerg.* **1980**, *594*, 53−84.
(49) Iyanagi, T.; Xia, C.; Kim, J.-J. P. NADPH-Cytochrome P450 Oxidoreductase: Prototypic Member of the Diflavin Reductase Family. *Arch. Biochem. Biophys.* **2012**, *528*, 72−89.
(50) Ellis, H. R. The FMN-Dependent Two-Component Monooxygenase Systems. *Arch. Biochem. Biophys.* **2010**, *497*, 1−12.

DOI: 10.1021/acs.biomac.7b01706
Biomacromolecules XXXX, XXX, XXX−XXX